RSCPublishing Faraday Discussions

# UV–Responsive Cyclic Peptide Progelator Bioinks

SCHOLARONE™
Manuscripts

# UV-Responsive Cyclic Peptide Progelator Bioinks

**Andrea S. Carlini**[a,b,f]**, Mollie A. Touve**[b,f]**, Héctor Fernández-Caro**[b,i]**, Matthew P. Thompson**[b,c,d,f,g,h]**, Mary F. Cassidy,**[e] **Wei Cao,**[b,c,d,f,g,h] **and Nathan C. Gianneschi**[*a,b,c,d,f,g,h]

[a]Department of Chemistry & Biochemistry, University of California, San Diego, La Jolla, California 92093, United States.

[b]Department of Chemistry, [c]Department of Materials Science & Engineering, [d]Department of Biomedical Engineering, [e]Department of Chemical and Biological Engineering, [f]International Institute for Nanotechnology, [g]Chemistry of Life Processes Institute, and [h]Simpson Querrey Institute, Northwestern University, Evanston, Illinois 60208, United States.

[i]Centro Singular de Investigación en Química Biolóxica e Materiais Moleculares (CIQUS) and Departamento de Química Orgánica, Universidade de Santiago de Compostela, Rúa Jenaro de la Fuente s/n, 15782, Santiago de Compostela, Spain.

Email: nathan.gianneschi@northwestern.edu

*Supporting Information Placeholder*

## Abstract

We describe cyclic peptide progelators which cleave in response to UV light to generate linearized peptides which then self-assemble into gel networks. Cyclic peptide progelators were synthesized, where the peptides were sterically constrained, but upon UV irradiation, predictable cleavage products were generated. Amino acid sequences and formulation conditions were altered to tune the mechanical properties of the resulting gels. Characterization of the resulting morphologies and chemistry was achieved through liquid phase and standard TEM methods, combined with matrix assisted laser desorption ionization imaging mass spectrometry (MALDI-IMS).

## 1 Introduction

UV-responsive biomaterials are commonly employed in printing technologies to make artificial tissues and biomimetic substrates because of the high spatial resolution and tunable wavelength of activation lasers. Such bioinks have been employed in projection-based,[1] sterolithography,[2] and laser-assisted[3] three-dimensional (3D) printing. Rigorous control over assembly crosslinking density and feature sizes can

enable the exploration of nL-scale reactions, either within a defined boundary or between reagents across a diffusion-controlled barrier. However, current strategies generally rely on inks that produce feature sizes controlled entirely by the laser aperture. Thus, 3D printed tissue scaffolds[4-7] do not recapitulate the architectural complexity exhibited by most biological scaffolds, such as the fibrous (10-300 nm diameter) extracellular matrix (ECM).[8,9] Notably, the ECM exists as a porous, delicate network of peptide nanofibers entangled to generate a weak physical gel.

More recently, four-dimensional (4D) printing technologies, in which position ($x$, $y$, $z$) and chemical composition are controlled using shape-memory and/or transforming polymers that respond to various stimuli (e.g. irradiation,[10] temperature,[11] humidity,[12] electricity,[13] magnetism,[14] and solvation[15]), have expanded the behavioral diversity of printed materials. The use of UV-responsive bioinks for 4D printing of patterned self-assembling scaffolds with nanoscale resolution are of particular interest for designing microfluidic devices, bioarrays, and mimetic biological interfaces.[16]

We propose a strategy to reverse-engineer a biomimetic ECM through controllable printing of soft material inks. Peptides were selected as the base component of our ink material due to their inherent biocompatibility, absolute sequence control lending reproducible manufacturing, and a toolbox of commercially available amino acids which allows the expansion of sequence modularity. Furthermore, we were inspired by synthetic and processing efforts to control peptide morphologies[17-19] and their spatial organization[20-22] because of their inherent capacity to self-assemble through ionic crosslinking, amphiphilic, and/or π-π stacking interactions. As such, a UV-responsive ink that produces a local and patterned array of these active peptides, which themselves produce hierarchical assemblies, will enable "4D" printing of a biomimetic ECM.

Herein, we present the development of a photocleavable peptide that is sterically constrained to prevent gelation prior to treatment with UV light (**Figure 1**). This stimuli-responsive peptide ink selectively generates macromolecular complexes with nanoscale features (**Figure 1a-c**). We show that liquid cell transmission electron microscopy (LCTEM) can be used to simultaneously activate the UV-responsive nitrophenyl substrate and probe self-assembly in real time. Matrix-assisted laser desorption ionization imaging mass spectrometry (MALDI-IMS) characterization provides a further means for chemically verifying that the e⁻ beam can be used as a source of inducing cleavage without initiating damage (**Figure 1d**). Our method for printing complex scaffolds by design, as opposed to homogenous traces in conventional practices, may provide nanoscale features necessary for the study and construction of biological systems.
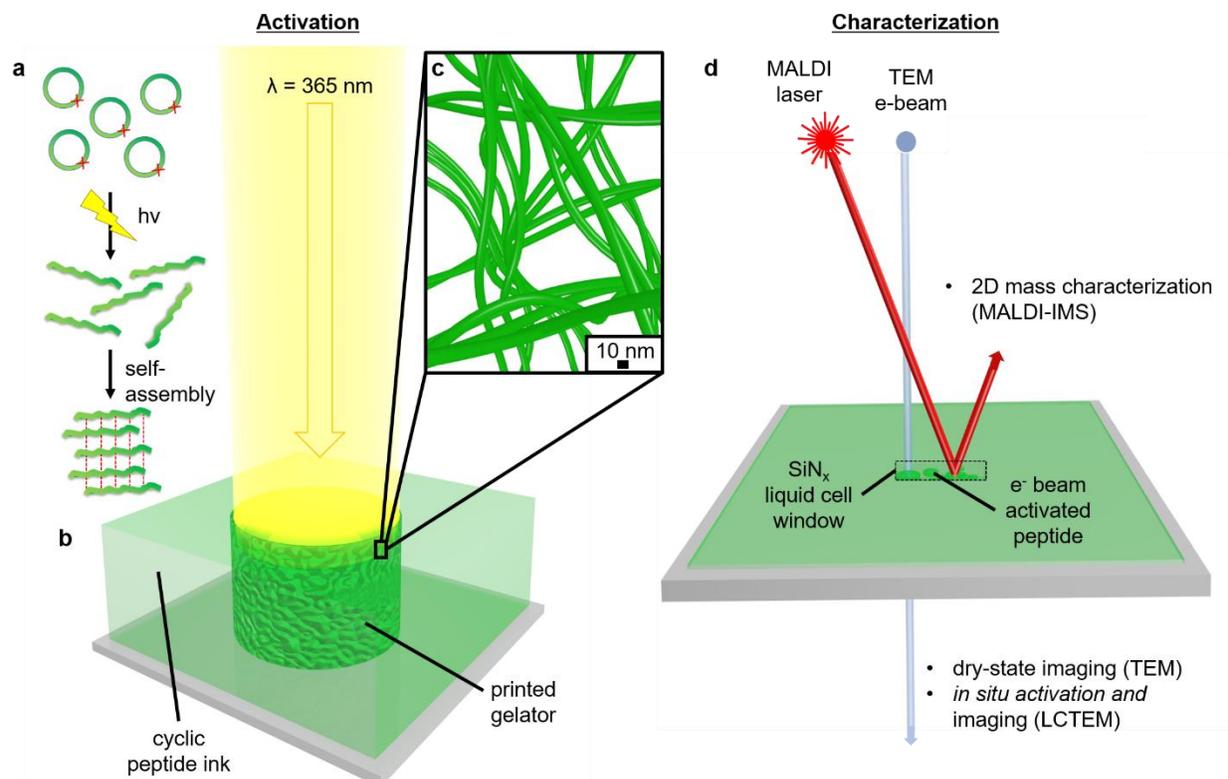
**Figure 1. Schematic of UV-responsive ink activation and characterization. a-b)** Sterically constrained cyclic peptide linearize in response to UV activation, and self-assemble through amphiphilic interactions. **b)** Bulk scale activation from a solution of cyclic peptide ink provides a means for 4D printing of an ECM-like gel comprised of (**c**) entangled nanofiber networks. **d)** Characterization of silicon nitride ($SiN_x$) chip surfaces to explore morphology by transmission electron microscopy (TEM) and chemical signatures by matrix-assisted laser desorption ionization imaging mass spectrometry (MALDI-IMS).

## 2. Results and Discussion

### Design of amphiphilic peptide as gelling ink template

A variety of short peptides sequences are reported to assemble as nanofibers such as rP11, KLD-12, MAX1 RADA16, FF dipeptide, KFE8, and $OVA_{257-264}$.[23-25] Many of these sequences possess primary amines from an unprotected N-terminus or Lys R-group. This moiety can react with UV active *o*-nitrobenzyl groups,[26] causing potential side reactions that disrupt overall capacity to self-assemble into ordered structures. Therefore, the peptide-based inks generated in this study utilized a core gelator sequence free of Lys residues and N-capped with acetyl groups. We designed a new gelling peptide sequence that blends the amino acid sequences possessed by small hydrophobic Fmoc-FF dipeptide[27] and more hydrophilic stimuli-responsive PhAc-FFAGLDD,[18] to generate an amphiphilic gelator composed of nonionic R-groups, Ac-

GFFFLGSGS (**Figure 2** and **Figure S1**). The GSGS repeat has been used in our lab to provide a neutral linker for increasing peptide-polymer amphiphile solubility in aqueous solutions.[28] This unique nonionic, amphiphilic gelator sequence formed a physical gel in which unimer packing was influenced by both peptide and salt concentration, as well as applied shear forces (**Figure 2a**). TEM under dilute conditions revealed fibrous morphology akin to native ECM (**Figure 2b**), and concentrated samples in aqueous mixtures of $H_2O$/acetonitrile or PBS/acetonitrile (90:10 %v/v) formed viscoelastic gels, exemplified by larger storage (G') than loss (G'') moduli (**Figure 2c-d**). Additionally, greater angular frequency independence in the salt-containing sample demonstrated increased resistance to flow compared to salt-free peptide solutions. Finally, this gelator exhibited shear-thinning capacity, a characteristic property of self-assembling peptides.
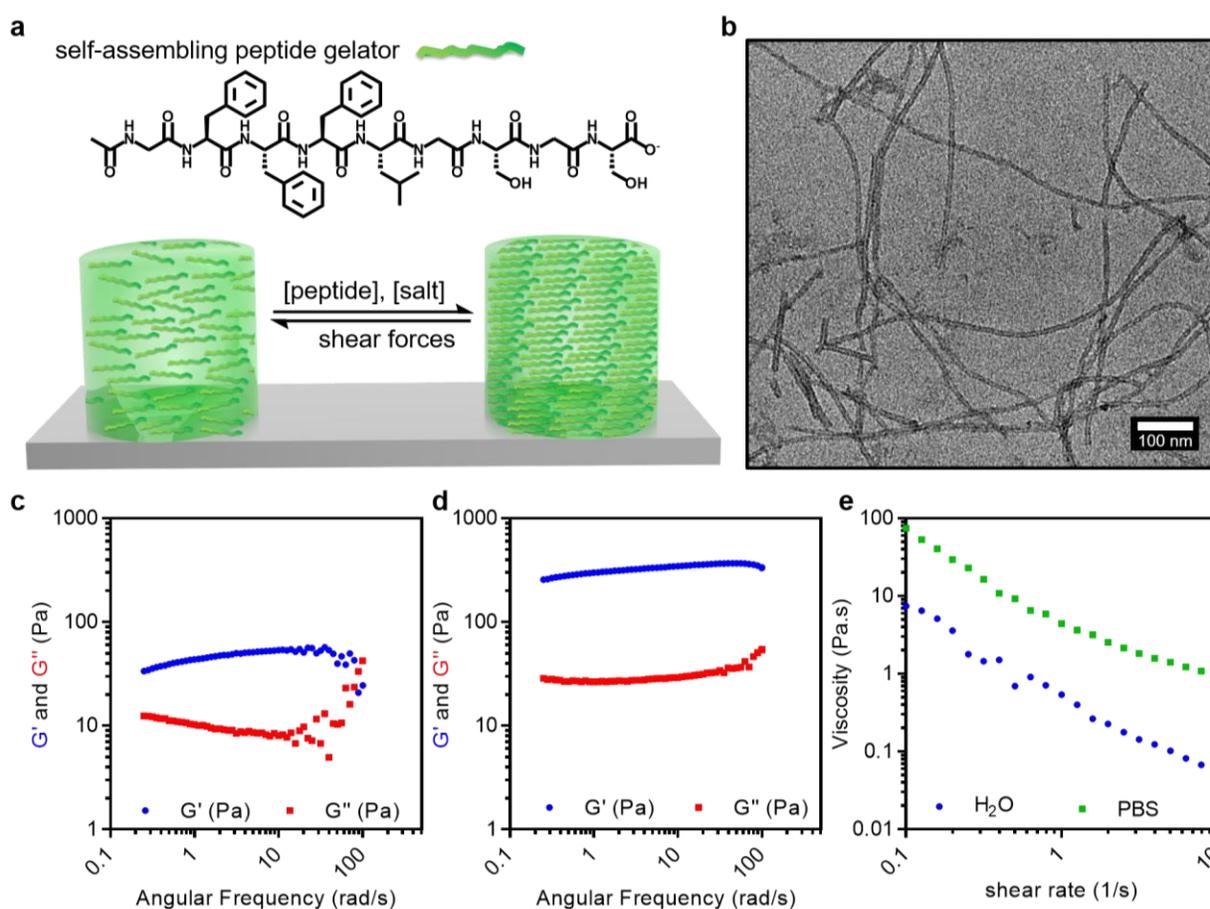


**Figure 2. Design of self-assembling peptide gelator. a**) Schematic of self-assembling peptide gelator, with amino acid sequence Ac-GFFFLGSGS, showing that peptide and salt concentration are directly correlated to unimer packing and shear forces induce disassembly. **b**) Fibrous morphology of gelator (100 µM) by dry state TEM. **c-e**) Bulk scale rheological characterization of gelator (15 mg/mL). Frequency sweeps showing storage (G') and loss (G'') moduli of gelator prepared in (**c**) $H_2O$ (pH 6.4) and (**d**) 1x PBS (pH 7.4). (**e**) Corresponding complex viscosity as a function of shear rate.

**Identification of a responsive moiety with predictable UV cleavage products.**

A multitude of UV cleavable amino acids have been reported in the literature, such as 2-nitrophenylglycine (NPG),[29] expanded *o*-nitrobenzyl linker,[30] *o*-nitrobenzyl caged phenol,[31] *o*-nitrobenzyl caged thiol,[32] nitroveratryloxycarbonyl (NVOC) caged aniline,[33] *o*-nitrobenzyl caged selenides,[34] bis-azobenzene,[35] coumarin,[36] cinnamyl,[37] spiropyran,[38] 2-nitrophenylalanine (2-nF),[39] and 3-amino-3(2-nitrophenyl)propionic acid (ANP).[40,41] For the purpose of simplicity and scalability, we focused on commercially available nitrophenyl-based amino acids, as they are easily incorporated into the peptide sequence using SPPS without further modification. Initial systems utilized 2-nitrophenylalanine (2-nF), due to its low cost and sensitivity to UV light at 365 nm. Linear peptide sequences were synthesized and cyclized via N-to-C amidation through the N-terminal lysine amine and C-terminal carboxylic acid, to create **cyc(2-nF)** (**Figure S2**). To eliminate the presence of free amines and their subsequent reactivity with the activated nitrobenzyl group, the N-terminus was acetylated. Photoactivation of **cyc(2-nF)** yielded a viscous gel, demonstrating that self-assembly because of UV activation is possible. However, LCMS revealed a multitude of hydrophilic chemical species over time. Furthermore, the mass of these chemical species did not correlate with the predicted cleavage products proposed by Peters *et. al* for 2-nF amino acid bearing peptides.[39] Given the need for self-complementary peptide sequences to generate discrete morphologies and bulk physical gels, predictable and reliable photocleavage products are necessary.[25]

ANP was then selected as an alternative commercially available responsive moiety which achieves specific, single site peptide cleavage for reliable and reproducible macrocycle linearization.[42] Given the similarity in mass and expected HPLC peak retention time inherent to the cyclic precursor ink and its cleaved, linearized product, we developed a linear ink analogue, **lin(ANP)**, in which photocleavage was expected to release a short hydrophilic peptide linker and change the product peptide hydrophobicity (**Figure 3**). The linear analogue, **lin(ANP)**, with sequence Ac-GG(ANP)GFFFLGSGS (**Figure 3a**), was dissolved in an aqueous mixture of H$_2$O and ACN, and submitted to photocleavage at 365 nm for 4 hr. The proposed mechanism of photocleavage and side product formation in **Figure 3b** was based on the mechanism reported by Liang *et. al*.[42] Activation of the starting material (1) nitrophenyl moiety is accompanied by cleavage of the N-terminal amine, releasing the soluble Ac-GG linker, with subsequent rearrangement into an N-terminal nitroso compound (2). The dehydration product (3) and methanol adduct (4) were then generated. Notably, addition of methanol to the solution has been reported to push equilibrium towards a methyl ester compound for simpler product characterization. As such, all photocleavage reactions in this study were performed in the presence of a small quantity of methanol (~5 % v/v). HPLC analysis of the solution during revealed a mixture of compounds 1-4 after 1 hr, with convergence upon the methanol adduct after 3 hours (**Figure 3c**). Decreased solubility of cleaved **lin(ANP)** exhibited self-assembly into a

cloudy aggregate. Additionally, a distinct color change from clear to yellow was observed, indicative of the indolin-3-one cleavage product. Observed peak masses by electrospray ionization mass spectrometry (ESI-MS) agree with expected values (**Figure 3d** and **Figure S3**).
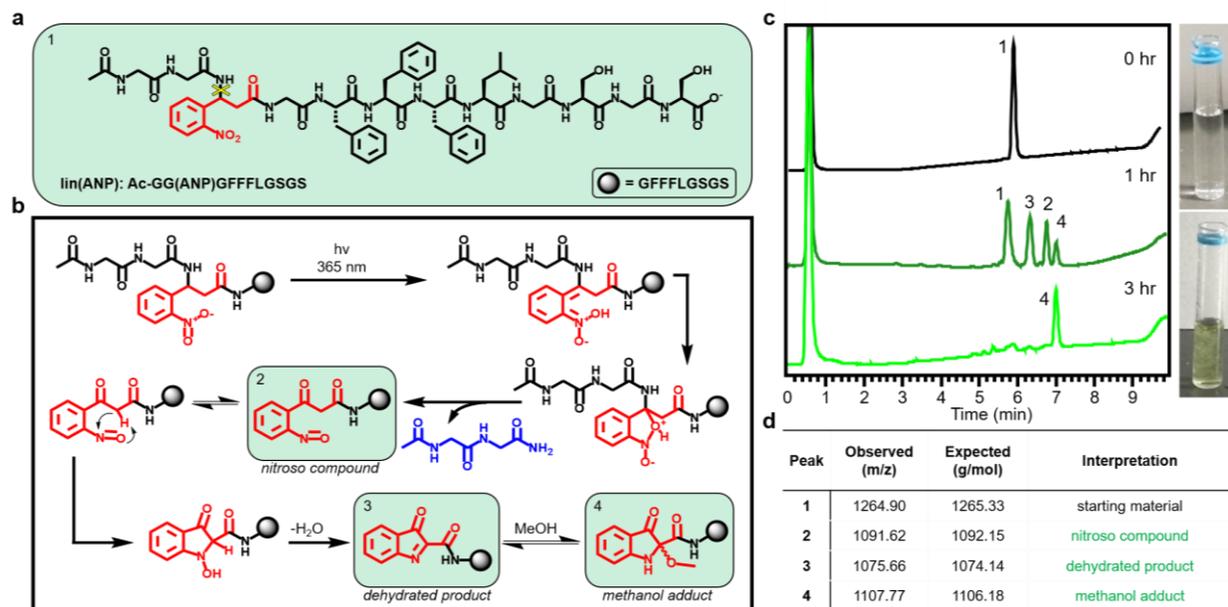


**Figure 3. Photoactivation of a linear ink analogue produces reliable cleavage products. a**) Linear ink analogue with photocleavable ANP residue. **b**) Proposed photocleavage mechanism showing conversion of the (1) starting material to a (2) nitroso compound, (3) dehydrated product, and (4) methanol adduct.[42] **c**) HPLC spectra vial pictures of linear ink analogue during cleavage at 0, 1, and 3 hr. Peaks labeled according to (**b**). **d**) Corresponding observed and expected mass spectra of peaks.

**Peptide macrocyclization to generate sterically constrained inks.**

Gelator macrocyclization presents a rapid, clean, and synthetically simple method for generating a structurally dynamic peptide ink (**Figure 4**). Peptides synthesized through SPPS were cleaved from 2-CTC resin with simultaneous deprotection of the Lys(Mtt) to generate the semi-protected peptide, Ac-K(ANP)GFFFLGS(otBu)GS(otBu) (**Figure 4a**). Amide bond formation between the C-terminal carboxylate and Lys R-group amine occurred under dilute conditions (500 µM in DMF) for 24 hr to generate the semi-protected macrocyclic peptide. Final amino acid deprotection yielded **cyc(ANP)**. LCMS analysis shows a characteristic shift in peak retention from 6.4 min to 7.3 min, indicative of an increase in peptide hydrophobicity (**Figure 4b**). Additionally, no dimerization was observed. Corresponding ESI mass spectra of peptide peaks at 0 hr and 24 hr reveals a loss of $H_2O$ [M-18] upon cyclization, which corresponds to the expected masses (**Figure 4c-d**). Finally, **cyc(ANP)** was purified by preparatory phase HPLC.
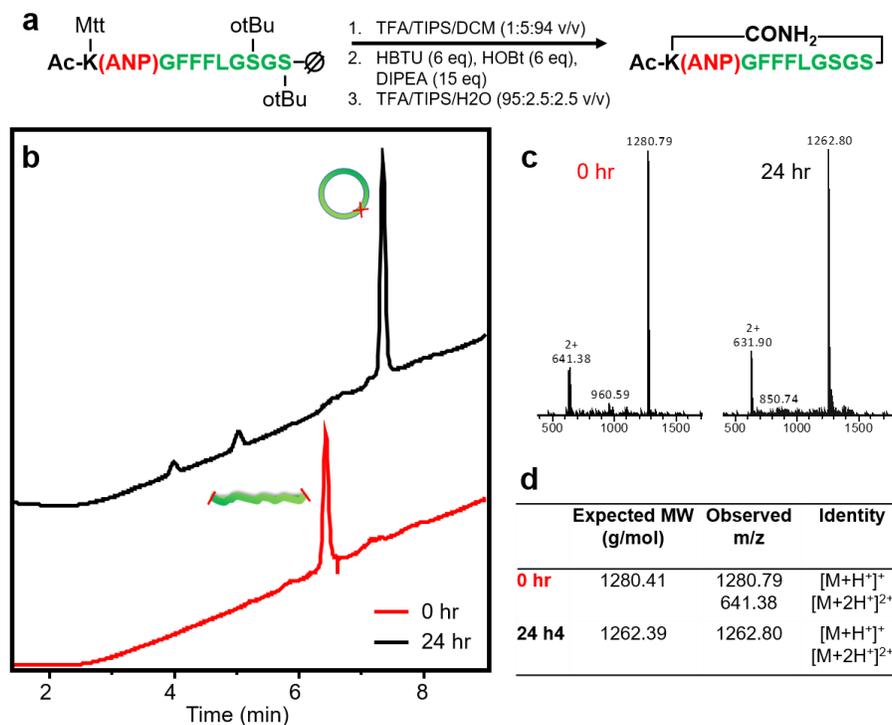
**Figure 4. Peptide macrocyclization to generate photocleavable inks. a**) Synthetic scheme for generation of macrocycle, cyc(ANP) from resin-bound peptide. Synthesis involved (1) cleavage from resin and Lys(Mtt) deprotection, (2) amide bond formation between the Lys R-group amine and C-terminal carboxylate under dilute conditions (500 µM in DMF), and (3) serine R-group deprotection. **b**) LCMS of fully deprotected peptides at 0 hr and 24 hr of cyclization. **c**) Corresponding ESI mass spectra. **d**) Table of expected and observed masses with corresponding mass identities.

## Photocleavage of a UV-responsive cyclic peptide ink.

To test the mechanism of photocleavage, our ink was dissolved in a high concentration of organic solvent to ensure that starting material and products remained dispersed in solution during UV treatment, and that self-assembly did not slow the reaction (**Figure 5**). A bulk solution of **cyc(ANP)** in $H_2O$/ACN/MeOH (50:45:5 %v/v) was submitted to photocleavage (365 nm) for 4 hr and monitored for cleavage products 2, 3, and 4 (**Figure 5a**). HPLC coupled with ESI-MI analysis of peaks revealed at all three compounds were present during UV treatment, demonstrating that synthetic and structural differences between **lin(ANP)** and **cyc(ANP)** do not affect the reaction (**Figure 5b**). After 4 hours, the methanol adduct (4) was the primary photocleavage product present in solution. Experimentally observed peak masses agree with expected values (**Figure 5c**). Notably, linearized photocleavage products were more hydrophilic than the cyclic precursor ink, as shown by their decreased retention times. We hypothesized that increased solvation in aqueous solution will enable gel assembly of linearized photocleavage products.
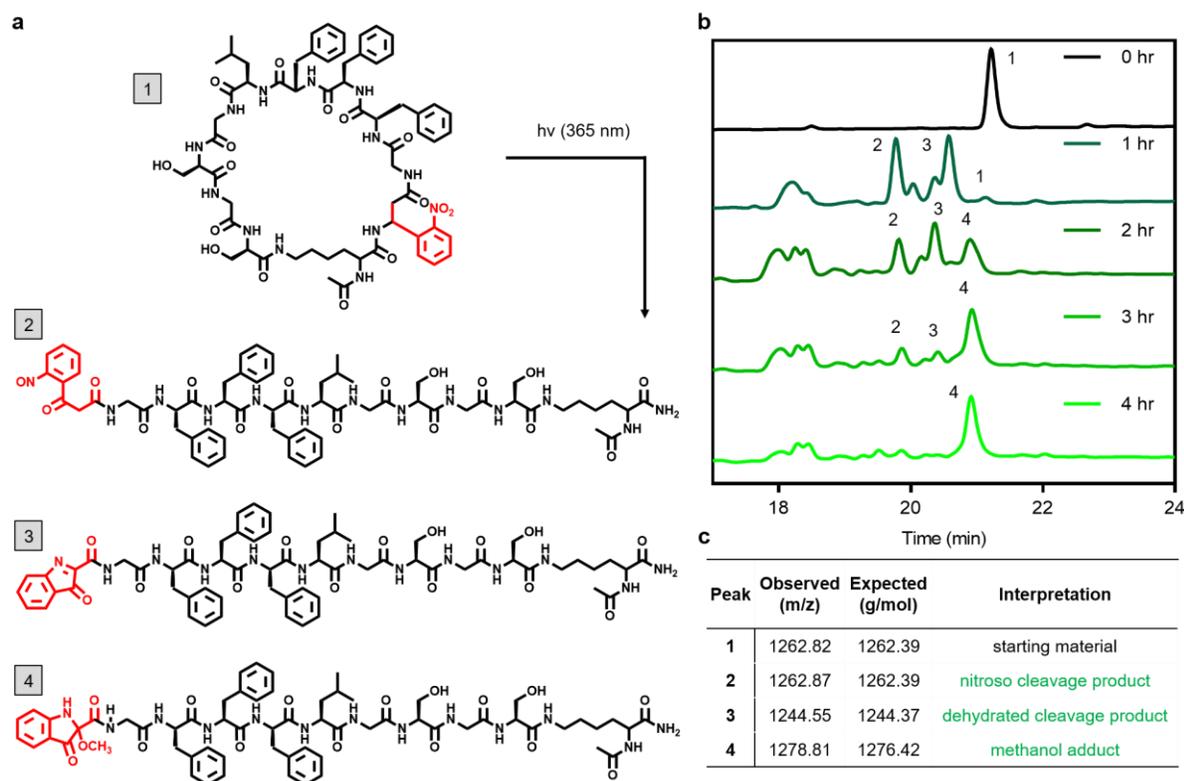
**Figure 5. UV Cleavage of cyclic peptide ink. a**) Chemical structures of cyclic peptide (1) proposed cleavage products (2, 3, and 4). **b**) HPLC spectra of UV-treated ink after 0, 1, 2, 3, and 4 hr of UV (365 nm) treatment, with relevant peaks labeled. **c**) Corresponding ESI mass spectra of collected peaks from (**b**).

Given the high hydrophobicity of **cyc(ANP)**, dissolution directly into $H_2O$ was not possible. Various conditions were explored, with formulations 1 and 2 shown in **Figure 6**. In formulation 1, peptide was dissolved in a mixture of $H_2O$/ACN (66:33 %v/v), heated to evaporate off ACN, and cooled to room temperature. Slow aggregation of the peptide in solution resulted in a slurry (**Figure 6a**). Dry state TEM revealed the presence of micron scale amorphous **cyc(ANP)** aggregates (**Figure 6b**). Treatment of the slurry solution with UV light and subsequent linearization increased peptide solubility, yielding a visible gel in solution. The resulting TEM morphology of shows large elongated ribbon structures (~100 nm thick), significantly thicker than that of **linGelator** (~12 nm thick). To improve solubility, Formulation 2 involved dissolving **cyc(ANP)** in a mixture of $H_2O$/ACN/AcOH (85:10:5 %v/v) with heating, which produced a clear free-flowing solution (**Figure 6c**). The size of **cyc(ANP)** aggregates was reduced from micro- to nano-scale structures (~200 nm) by TEM (**Figure 6d**). In this improved formulation, UV treatment also produced a gel, but with fibrous morphology and thickness (~10-15 nm) akin to that of **linGelator**. These results demonstrate that ink formulation significantly impacts the product morphologies, but it does not disrupt the

overall capacity to self-assemble as a gel in response to photocleavage. Furthermore, we show that resulting gel morphology can be manipulated solely from ink formulation alone. As the linearized photocleavage product is more hydrophilic than the cyclic precursor, we suspected that solvent exchange into pure $H_2O$ or PBS after gel formation may be a viable means for 4D printing of ECM mimics for biological applications. Alternatively, modified peptide sequences which produce more water-soluble inks could eliminate the need for these harsh formulation conditions.
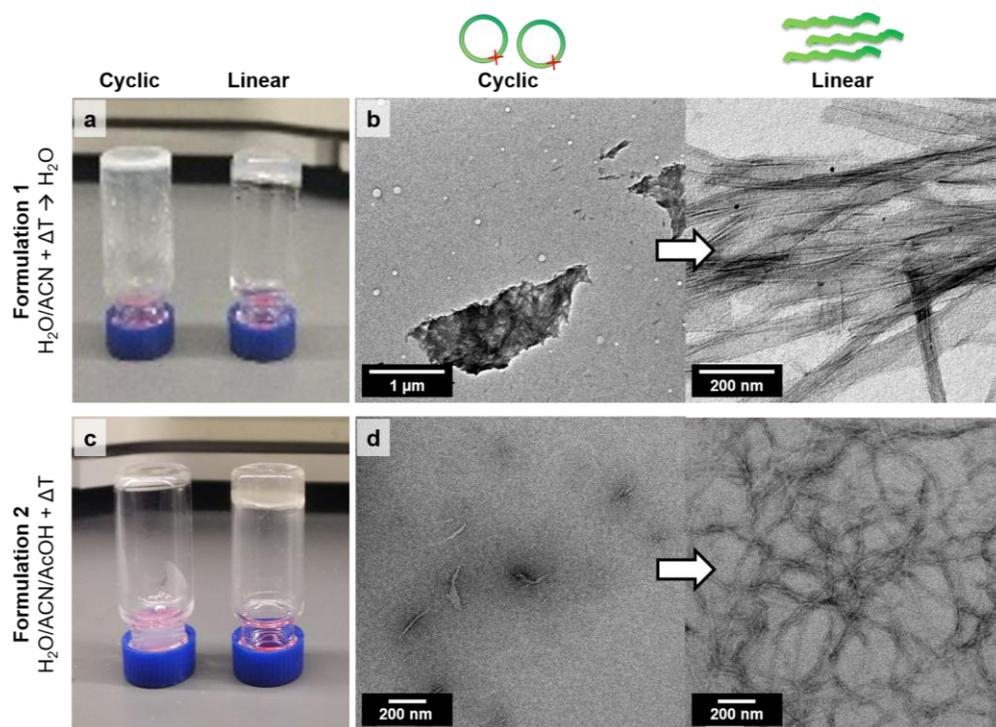


**Figure 6. Morphological analysis of cyc(ANP) ink with and without UV treatment. a-b**) Formulation 1 conditions: Dissolution in $H_2O$/ACN (66:33 %v/v) with heating (60 °C), and heating (80 °C) to remove acetonitrile. (**a**) Picture of vial flips from (left) untreated and (right) treated peptide sample (10 mg/mL). (**b**) Corresponding dry state TEM of (left) untreated and (right) treated samples (500 µM). **c-d**) Formulation 2 conditions: Dissolution in $H_2O$/ACN/AcOH (85:10:5 %v/v) with heating (60 °C). Neutralization to pH 6.4 with $NH_4OH$. (**c**) Picture of vial flips from (left) untreated and (right) treated peptide sample (10 mg/mL). (**d**) Corresponding dry state TEM of (left) untreated and (right) treated samples (500 µM).

A modified gelator (**linGelator-II**: GFFFLGSGSGS) was generated for increased solubility by removing the N-terminal acetyl group and added extra GS sequence (**Figure S4**). Given the zwitterionic nature of this

new gelator, which contains a cationic N-terminal amine and anionic C-terminal carboxylate, overall solubility was increased in water after using a pH-switch from pH 10 to pH 6.4, negating the need for ACN with this gelator. Conventional dry-state TEM confirmed that **linGelator-II** forms well-defined fibrous networks (**Figure 7**).

**Utilizing MALDI-IMS to verify chemical identities of dry-state TEM samples.**

Validating chemical composition is an important analytical component in the generation of a novel nanomaterial. For materials that are generated in solution, various standard analytical techniques are available for probing chemical identities (e.g., nuclear magnetic resonance, size exclusion chromatography). However, few techniques exist for probing the chemistry of materials that are dried-on or covalently bound to a surface, especially at low analyte concentrations. We previously demonstrated the use of MALDI-IMS to directly probe the chemical identities of substances dried on silicon nitride ($SiN_x$) chip surfaces.[43] Specifically, using MALDI-IMS, thousands of mass spectra could be generated across a $SiN_x$ TEM chip surface to determine chemical identities of materials generated *in situ* during LCTEM experiments. With this technique, we can verify whether the observed structures possess a claimed chemical identity. Analogous to energy-dispersive X-ray (EDX) and electron energy loss spectroscopy (EELS) analysis of S/TEM samples, here we were interested in directly analyzing chemical signatures of macromolecular assemblies that had been imaged by TEM, either in the dry state by conventional TEM, or in a hydrated state by LCTEM.

Similar to conventional dry-state TEM sample preparation on copper grids with carbon films, an aliquot of **linGelator-II** was deposited onto a $SiN_x$ chip, then the solution was allowed to dry. Dry-state TEM imaging of the $SiN_x$ chip showed well-defined fibers, without staining, identical to those observed by conventional dry-state, uranyl acetate stained TEM (**Figure 7a-b**). After imaging, the chip was attached to an indium-tin-oxide (ITO) slide, evenly coated with matrix, then analyzed by MALDI-IMS. The mass spectra verified that the fiber structures observed on the chips possessed the expected mass:charge signature (1089 Da) (**Figure 7c-e**). By comparing the relative intensities of a specific *m/z* value across the generated MALDI-IMS map, we can gain information on the abundance of the material, which can be important when generating materials with questionable purity.
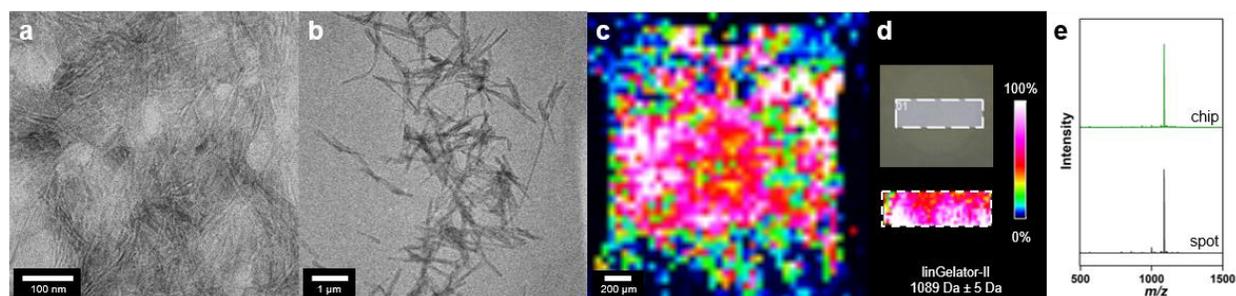
**Figure 7. Dry-state TEM imaging and MALDI-IMS mapping of linGelator-II**. **a)** Conventional dry-state, uranyl acetate stained TEM image of **linGelator-II** fibers. **b)** Dry-state, unstained image of **linGelator-II** fibers on a $SiN_x$ chip. **c)** MALDI-IMS map of the surface of the chip shown in (**b**) with mass filter for **linGelator-II** (1089 Da +/- 5 Da) applied. **d)** Optical picture of **linGelator-II** spot on ITO slide with MALDI-IMS measurement region outlined (top) and corresponding MALDI-IMS map with mass filter for **linGelator-II** applied (bottom). **e)** Overall MALDI mass spectra for **linGelator-II** spot (bottom) and chip surface (top).

### Use of an electron beam for nanoscale printing *in situ*

To analyze real-time morphology changes of the peptide inks, we hypothesized that the electron beam of a transmission electron microscope (TEM) could act as a stimulus to activate the more labile components of the **cyc(ANP)** peptide (i.e., the ANP UV-responsive moiety) and, as a result, promote the growth of nanoscale assemblies observable by TEM.[44] For this imaging experiment, a solution of **cyc(ANP)** was irradiated under low electron flux conditions, where the amount of electrons irradiating a unit area over time ($e^-/Å^2s$) is kept to a minimum to mitigate beam-induced damage to the peptide structures and the solvent (**Figure 8**).[44-46] All LCTEM imaging was conducted at the corners of the liquid cell, where the window thickness is minimal, to detect and observe the formation of these structures which possess minimal TEM contrast. Immediately upon exposure of the electron beam on the peptide solution under low flux conditions (0.1 $e^-/Å^2s$), low-contrast structures were observed to form and grow with increasing contrast for 2-3 min within the irradiated regions of the window (**Figure 8a-d**). As macromolecular structures assembled and grew during imaging, they were not observed to move along the surface of the window region. We suspect that limited diffusion in the confined environment of the liquid cell, as well as potential interaction with the $SiN_x$ surface, provided an immobilizing environment.

Given that we were able to observe the formation of structures from a peptide solution by LCTEM, we wanted to probe the chemistry of these structures to elucidate whether the formed architectures are from the same cleavage event which occurs during UV irradiation, or if the architectures are instead forming as a result of a different route of cleavage, as might be expected because of a change in the type of radiation utilized. To do this, we chemically analyzed the surface of the LCTEM chips after the *in situ* experiment

by MALDI-IMS. After LCTEM, the two chips were gently pried apart and the sample solution was dried. The chips were mounted onto an ITO slide, evenly coated with matrix, then analyzed by MALDI-IMS. The mass for **cyc(ANP)** was present across the surface of the chips (1263 *m/z*) (**Figure 8e**). Interestingly, we did not observe the UV cleavage product, as discussed above (**Figure 8e-k**). Rather, the new masses obtained were approximately 400 *m/z* lower than that of the starting material, suggesting an altered mechanism of chemical cleavage when stimulated with an electron beam. Colorized mapping of these new masses (880 +/- 5% *m/z*) reveal two small localized regions (~250 nm x 250 nm) of this material near the center of the chip on both chip surfaces of the liquid cell assembly. We suspect that this new mass corresponds to electron beam-activated peptide within the window region, and that the displacement of this material away from the centered window regions of the chips occurred during chip separation prior to MALDI-IMS analysis. Altogether, we observe that the electron beam can successfully and locally activate peptides bearing the ANP-responsive moieties, but the mechanism of activation by a TEM electron beam is clearly different from when UV light is utilized as a stimulus.
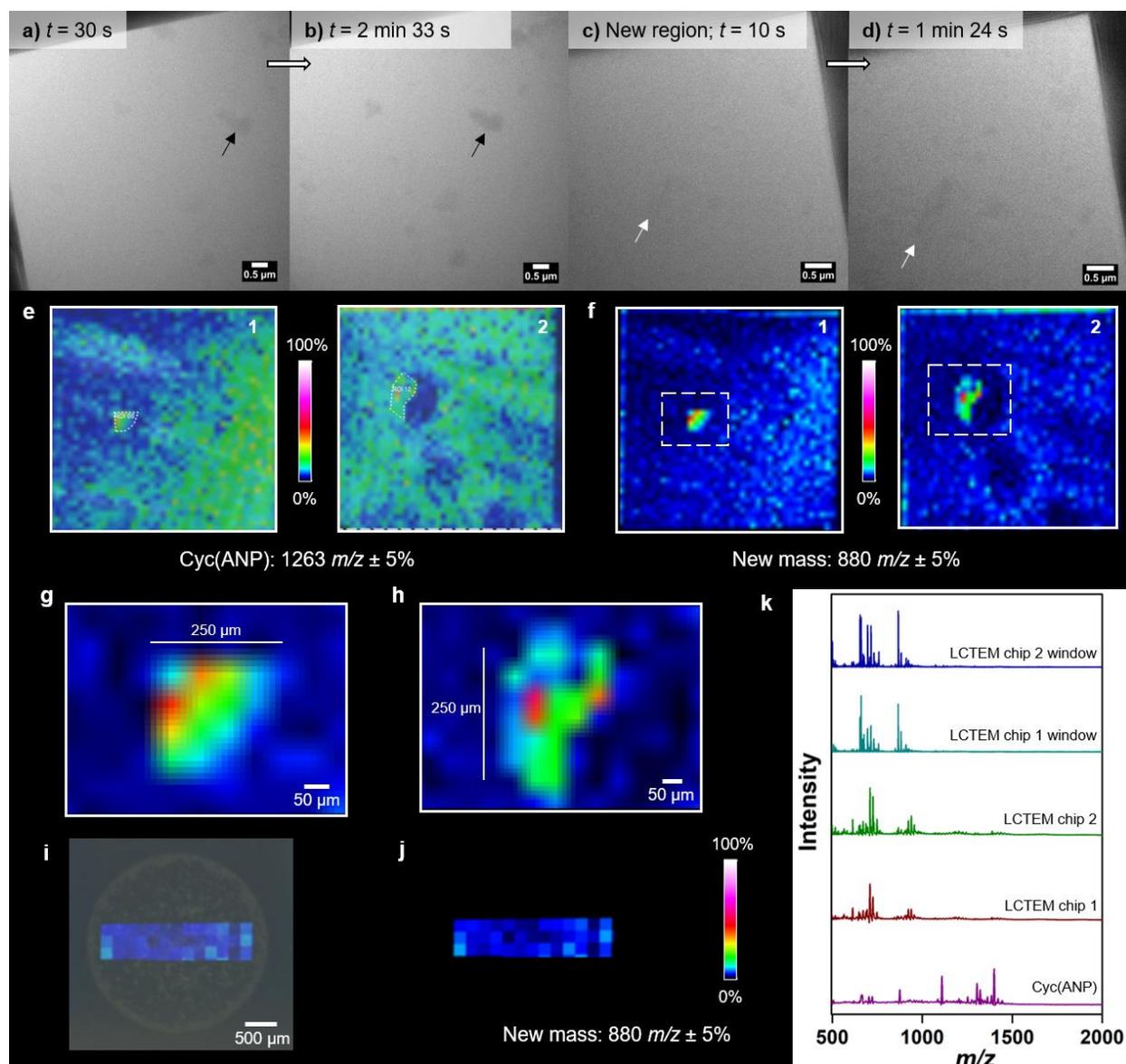
**Figure 8. Activating peptide assembly with the electron beam of a TEM. a-b**) LCTEM snapshots of a region of a liquid cell containing **cyc(ANP)**, where $t = 0$ is when the region imaged was first irradiated with the electron beam. Images at (**a**) 30 s and (**b**) 2 min 33 s are shown. Arrows point out one structure change over time. Electron flux = 0.1 e⁻/Å²s. **c-d**) Snapshots of another region of the same liquid cell at (**c**) 10 s and (**d**) 1 min 24 s. **e-f**) MALDI-IMS 2D mapping of the two chip surfaces from the liquid cell experiment shown in (**a-d**). Applied mass filter for (**e**) **cyc(ANP)** (1263 +/- 5%) and (**f**) a new previously unobserved mass, (880 +/- 5%). **g**) Zoom-in of region of interest on chip surface shown in (**f**, left). **h**) Zoom-in of region of interest on chip surface shown in (**f**, right). **i**) Optical picture and MALDI-IMS 2D map overlay of a dried spot of UV peptide. **j**) 2D map overlay only of the dried spot of **cyc(ANP)** shown in (**i**). **k**) MALDI spectra for **cyc(ANP)** (purple), entire surface of chip 1 (red), entire surface of chip 2 (green), window of chip 1 (teal), window of chip 2 (blue).

# 3. Summary and Conclusion

The results presented herein validate our hypothesis for conformational steric hindrance as a method of triggering a bioink. We demonstrate with UV activation that bulk scale and localized self-assembly, respectively, was possible, with predictable cleavage products. The required adjustments in peptide chemistry highlight the importance that controlled cleavage can have on resulting morphologies. In addition to novel ink generation, after verifying fiber morphologies by dry-state TEM, MALDI-IMS can be utilized to probe and confirm the chemical identities of the self-assembled architectures at high spatial resolution and sensitivity, showing that MALDI-IMS can be extended as a more routine method of verification for nanoscale assemblies on surfaces and surface localized patterns more generally. We suggest that MALDI-IMS mapping is a powerful method for adding chemical information, or "color" to the otherwise purely morphological information of grayscale TEM images. Further, current 3D printing technologies to generate tissue scaffolds, such as porous gel networks, are traditionally defined by the user-defined scaffold design and printer specifications. Our strategy introduces a new method for printing of complex features without the need for increasing 3D print model complexity or printers with higher UV laser resolution. This may be an interesting avenue to explore multilayered 4D printing of variable morphologies using the **cyc(ANP)** ink or synthetically modified analogues. We envision these materials will be useful in nanolithography applications for generating microfluidic devices, and artificial tissue scaffolds for studying single cell or protein reactions.

## Conflicts of Interest

The authors declare no conflicts of interest.

## Acknowledgements

# References

1.      Xue D, Wang Y, Zhang J, Mei D, Wang Y, Chen S. ACS Applied Materials & Interfaces. 2018;10(23):19428-35.
2.      Zhou X, Zhu W, Nowicki M, Miao S, Cui H, Holmes B, Glazer RI, Zhang LG. ACS Applied Materials & Interfaces. 2016;8(44):30017-26.
3.      Lim KS, Schon BS, Mekhileri NV, Brown GCJ, Chia CM, Prabakar S, Hooper GJ, Woodfield TBF. ACS Biomaterials Science & Engineering. 2016;2(10):1752-62.
4.      Yan Y, Chen H, Zhang H, Guo C, Yang K, Chen K, Cheng R, Qian N, Sandler N, Zhang YS, Shen H, Qi J, Cui W, Deng L. Biomaterials. 2019;190-191:97-110.
5.      Oladapo BI, Zahedi SA, Adeoye AOM. Composites Part B: Engineering. 2019;158:428-36.
6.      Contessi Negrini N, Bonetti L, Contili L, Farè S. Bioprinting. 2018;10:e00024.
7.      He Y, Yang F, Zhao H, Gao Q, Xia B, Fu J. Sci Rep. 2016;6:29977.
8.      Guo X, Hutcheon AEK, Melotti SA, Zieske JD, Trinkaus-Randall V, Ruberti JW. Invest Ophthalmol Vis Sci. 2007;48(9):4050-60.
9.      Bancelin S, Aimé C, Gusachenko I, Kowalczuk L, Latour G, Coradin T, Schanne-Klein M-C. Nature Communications. 2014;5:4920.
10.     López-Valdeolivas M, Liu D, Broer DJ, Sánchez-Somolinos C. Macromol Rapid Commun. 2018;39(5):1700710.
11.     Han D, Lu Z, Chester SA, Lee H. Sci Rep. 2018;8(1):1963.
12.     Sydney Gladman A, Matsumoto EA, Nuzzo RG, Mahadevan L, Lewis JA. Nature Materials. 2016;15:413.
13.     Shin SR, Li Y-C, Jang HL, Khoshakhlagh P, Akbari M, Nasajpour A, Zhang YS, Tamayol A, Khademhosseini A. Adv Drug Del Rev. 2016;105:255-74.
14.     Zhao X, Kim J, Cezar CA, Huebsch N, Lee K, Bouhadir K, Mooney DJ. Proceedings of the National Academy of Sciences. 2011;108(1):67-72.
15.     Shin D-G, Kim T-H, Kim D-E. International Journal of Precision Engineering and Manufacturing-Green Technology. 2017;4(3):349–57.
16.     Carbonell C, Braunschweig AB. Acc Chem Res. 2017;50(2):190-8.
17.     Carlini AS, Braden RL, Luo C, Christman KL, Gianneschi NC. Nature Communications. *in press*.
18.     Kalafatovic D, Nobis M, Javid N, Frederix PWJM, Anderson KI, Saunders BR, Ulijn RV. Biomaterials Science. 2015;3(2):246-9.
19.     Bowerman CJ, Nilsson BL. J Am Chem Soc. 2010;132(28):9526-7.
20.     Adler-Abramovich L, Aronov D, Beker P, Yevnin M, Stempler S, Buzhansky L, Rosenman G, Gazit E. Nature Nanotechnology. 2009;4:849.
21.     Zhang S, Greenfield MA, Mata A, Palmer LC, Bitton R, Mantei JR, Aparicio C, de la Cruz MO, Stupp SI. Nature Materials. 2010;9:594.
22.     Adler-Abramovich L, Marco P, Arnon ZA, Creasey RCG, Michaels TCT, Levin A, Scurr DJ, Roberts CJ, Knowles TPJ, Tendler SJB, Gazit E. ACS Nano. 2016;10(8):7436-42.
23.     Habibi N, Kamaly N, Memic A, Shafiee H. Nano today. 2016;11(1):41-60.
24.     Chen J, Zou X. Bioactive Materials. 2019;4:120-31.
25.     Zhang H, Park J, Jiang Y, Woodrow KA. Acta Biomater. 2017;55:183-93.
26.     De Alwis Watuthanthrige N, Kurek PN, Konkolewicz D. Polymer Chemistry. 2018;9(13):1557-61.
27.     Raeburn J, Pont G, Chen L, Cesbron Y, Lévy R, Adams DJ. Soft Matter. 2012;8(4):1168-74.
28.     Blum AP, Kammeyer JK, Gianneschi NC. Chemical Science. 2016;7(2):989-94.
29.     England PM, Lester HA, Davidson N, Dougherty DA. Proceedings of the National Academy of Sciences. 1997;94(20):11025-30.

30.     Pellois J-P, Muir TW. Angew Chem Int Ed. 2005;44(35):5713-7.
31.     Shigenaga A, Tsuji D, Nishioka N, Tsuda S, Itoh K, Otaka A. ChemBioChem. 2007;8(16):1929-31.
32.     Liu G, Dong C-M. Biomacromolecules. 2012;13(5):1573-83.
33.     Roth-Konforti ME, Comune M, Halperin-Sternfeld M, Grigoriants I, Shabat D, Adler-Abramovich L. Macromol Rapid Commun. 2018;39(24):1800588.
34.     Eastwood AL, Blum AP, Zacharias NM, Dougherty DA. The Journal of organic chemistry. 2009;74(23):9241-4.
35.     Mba M, Mazzier D, Silvestrini S, Toniolo C, Fatás P, Jiménez AI, Cativiela C, Moretto A. Chemistry – A European Journal. 2013;19(47):15841-6.
36.     Shao Y, Shi C, Xu G, Guo D, Luo J. ACS Applied Materials & Interfaces. 2014;6(13):10381-92.
37.     Yan L, Yang L, He H, Hu X, Xie Z, Huang Y, Jing X. Polymer Chemistry. 2012;3(5):1300-7.
38.     Kotharangannagari VK, Sánchez-Ferrer A, Ruokolainen J, Mezzenga R. Macromolecules. 2011;44(12):4569-73.
39.     Peters FB, Brock A, Wang J, Schultz PG. Chem Biol. 2009;16(2):148-52.
40.     Umezawa N, Noro Y, Ukai K, Kato N, Higuchi T. ChemBioChem. 2011;12(11):1694-8.
41.     Grotenbreg GM, Nicholson MJ, Fowler KD, Wilbuer K, Octavio L, Yang M, Chakraborty AK, Ploegh HL, Wucherpfennig KW. The Journal of biological chemistry. 2007;282(29):21425-36.
42.     Liang X, Vézina-Dawod S, Bédard F, Porte K, Biron E. Org Lett. 2016;18(5):1174-7.
43.     Touve MA, Carlini AS, Gianneschi NC. *submitted*.
44.     Touve MA, Figg CA, Wright DB, Park C, Cantlon J, Sumerlin BS, Gianneschi NC. ACS Central Science. 2018;4(5):543-7.
45.     Woehl TJ, Abellan P. J Microsc. 2017;265(2):135-47.
46.     Schneider NM, Norton MM, Mendel BJ, Grogan JM, Ross FM, Bau HH. The Journal of Physical Chemistry C. 2014;118(38):22373-82.